Signal Processing: *Image Communication* 26 (2011) 518–533

Contents lists available at ScienceDirect

Signal Processing: *Image Communication*

journal homepage: www.elsevier.com/locate/image

Color image demosaicking: An overview

Daniele Menon *, Giancarlo Calvagno

Department of Information Engineering, University of Padova, via Gradenigo 6B, 35131 Padova, Italy

ARTICLE INFO

Article history:
Received 9 July 2009
Accepted 6 April 2011
Available online 4 May 2011

Keywords:
Demosaicking
Bayer pattern
Color filter array interpolation
Digital cameras

ABSTRACT

Demosaicking is the process of reconstructing a full-resolution color image from the sampled data acquired by a digital camera that apply a color filter array to a single sensor. This paper discusses the need of a color filter array and presents a survey of several techniques proposed to demosaicking. A comparison between the different methods is also provided, discussing their performances.

1. Introduction

In a typical digital camera each pixel is equipped with a sensor and a microlens that locally focuses the light away from circuitries and toward the photosensitive element of the sensor, usually a CMOS (*complementary metal oxide silicon*) or a CCD (*charge-coupled device*). Each CMOS active pixel sensor contains a photodetector and an active amplifier to measure the intensity of the light, while the CCD sensors rely on the electron-hole pair that is generated when a photon strikes silicon [1].

In a color digital camera the acquisition may require three sensors per pixel, each of them was sensitive to a particular wavelength. However, the positioning of the sensors is not straightforward. The sensors can be placed over a plane and the light entering the camera split in each pixel and projected onto each spectral sensor, but this solution is expensive and leads to some phase delay between the components. Another approach is to stack the color sensors on top of one another, as done in the Foveon cameras [2], but this arrangement increases the exposure time because the light has to penetrate three levels of silicon. Therefore, most of the digital cameras use a single sensor technique, with a grid of different color sensors, called *color filter array* (CFA). The most common pattern for the CFA has been introduced by Bayer [3], and it samples the green band using a quincunx grid, while red and blue are obtained by a rectangular grid, as shown in Fig. 1(a). In this way, the density of the green samples is twice than that of the red and blue channels. This arrangement has been used by most of the digital cameras, for instance in the Canon EOS 500D, Olympus E-450, Lumix DMC-FS12, FS62 and FS42, Sony Alpha 230, 330 and 380 and many others.

The Bayer pattern can be applied also using the subtractive primaries cyan, magenta, and yellow (CMY), as in the Kodak DSC620 × that have the advantage of being more sensitive to light. Another CFA configuration has been used by Sony in the DSC F828 digital camera, exploiting also the Emerald filter, while many companies use a cyan, magenta, yellow, and green array (CMYG), to provide a compromise between maximum light sensitivity and high color quality (such as in the Nikon Coolpix 990). Moreover, a yellow, cyan, green, unfiltered array originated at Hitachi is used by JVC in some of its video cameras. Several other arrangements have been proposed in the literature, such as the pattern shown in Fig. 1(b), presented in [4] or the new scheme introduced by Kodak [5], involving panchromatic pixels as in Fig. 1(c). Recently,

* Corresponding author. Tel.: +39 049 827 7641; fax: +39 049 827 7699.
E-mail addresses: menond@dei.unipd.it (D. Menon), calvagno@dei.unipd.it (G. Calvagno).

0923-5965/$ - see front matter © 2011 Elsevier B.V. All rights reserved.
doi:10.1016/j.image.2011.04.003

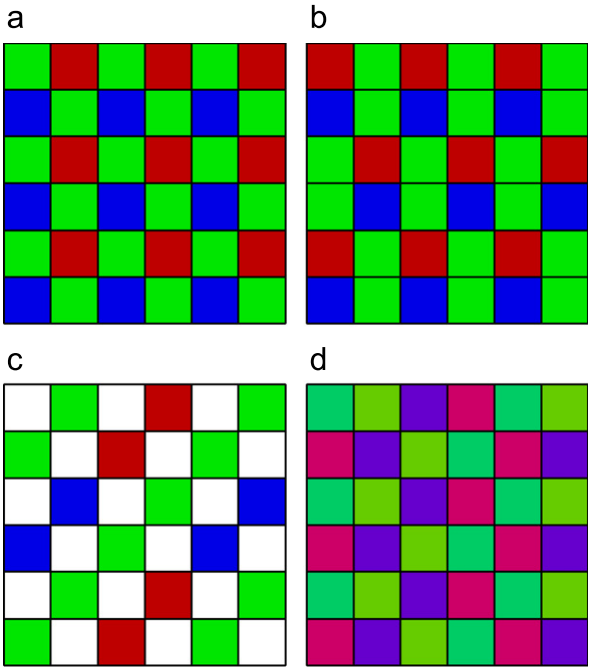

Fig. 1. Four arrangements for the color filter arrays: (a) the Bayer pattern [3]; (b) the pattern proposed in [4]; (c) the pattern proposed in [5] and (d) one of the patterns proposed in [6]. (For interpretation of the references to color in this figure legend, the reader is referred to the web version of this article.)

Hirakawa and Wolfe proposed new configurations where the sensors capture in each pixel a linear combination of the traditional red, green and blue components, in order to reduce the aliasing given by the sampling of the image [6]. One of these new patterns is shown in Fig. 1(d). Another novel CFA arrangement has been designed in [7], using a quantitative theory to find the optimal pattern that minimizes the reconstruction error resulting by a linear minimum mean square error estimation.

Due to the subsampling of the color components, an interpolation step is required in order to reconstruct a full color representation of the image. This process is called *demosaicking*. It is desirable that the reconstruction does not introduce visible artifacts that can affect the visual quality of the image. In particular, the aliasing component due to the sampling process can produce false colors in the most detailed regions of the image (see Fig. 2(a)), and zippering can be introduced near sharp edges, as in Fig. 2(b), due to the lattice structure of the CFA arrangement.

In literature, many demosaicking algorithms have been presented. As a matter of fact, the classical image interpolation methods, such as nearest-neighbor replication, bilinear interpolation and cubic spline interpolation, are not able to exploit the information given by the three color components jointly and do not provide good performances. Therefore better results are achieved by interpolation approaches specifically designed for the reconstruction of images sampled with a CFA.

In this paper we review most of the techniques considered for demosaicking. Since a huge number of approaches has been proposed, we subdivide them into five categories,

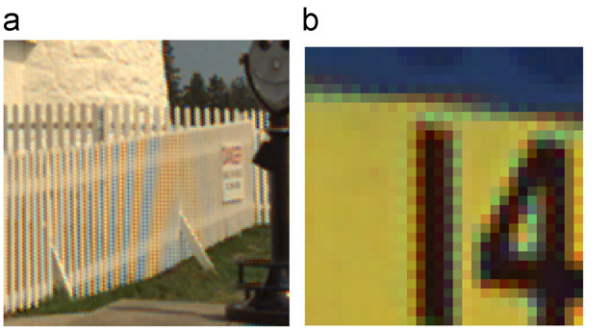

Fig. 2. Two examples of artifacts produced by a non-effective demosaicking technique: (a) false colors due to aliasing and (b) zippering.

namely heuristic methods, algorithms based on directional interpolations, frequency-domain approaches, wavelet-based methods, and reconstruction techniques. Moreover, we describe also some approaches proposed to perform demosaicking jointly with super-resolution, and algorithms for joint demosaicking and denoising. Although a classification into these categories could seem subjective, we think that it will be useful to read and follow this survey, without being thrown into confusion by the high number of the proposed algorithms. Other overviews about demosaicking complementary to this tutorial paper are given in [8–10].

In the following we focus our discussion on the reconstruction from images acquired with the Bayer patter, that is the most used CFA arrangement. However, in general some of the demosaicking algorithms developed for the Bayer pattern can be extended to other CFA configurations.

2. Heuristic methods

One commonly used assumption in color image processing is that the hue (the ratios between the color components) is smoother than the color components. Although this assumption only holds within the boundary of the objects in the image, it has been extensively used for demosaicking. Cok [11], after a reconstruction of the green channel with a bilinear interpolation, exploits it to reconstruct red and blue colors by interpolation of the red-to-green and blue-to-green ratios. Many other approaches follow a similar strategy, or, alternatively, find preferable to interpolate the differences of the color components, namely $R-G$, and $B-G$, instead of the color ratios [12]. Therefore, the reconstruction of the green channel becomes very relevant, since a good estimation of this component improves also the reconstruction of the red and blue values.

Many approaches are based on adaptive interpolation, where the reconstruction is performed in a directional way, and the interpolation is carried out along edges rather than across them. These algorithms use as horizontal and vertical edge-classifiers the gradient [13,14], the Laplacian operator [15–17], or the jacobian [18], and then they interpolate the green image along the selected direction. Among these methods, it is interesting to analyze the strategy proposed in [16,17]. In fact, Hamilton and

Adams observe that to assume smoothness of the color differences is equivalent to state that there is a correlation between the high-frequencies of the different color components and this correlation can be exploited for the reconstruction of the green channel. In fact, along a row (or a column) of the Bayer pattern, the green signal is subsampled with a factor of 2 and its Fourier transform is given by

$$G_s(\omega)=\frac{1}{2}G(\omega)+\frac{1}{2}G(\omega-\pi), \tag{1}$$

with $G(\omega)$ denoting the Fourier transform of the original green values. The low-pass filter $h_0=[0.5,1,0.5]$ used in bilinear interpolation cannot totally remove the aliasing component, but the resulting output can be corrected taking advantage of the information coming from the red and blue values. Considering a green–red row (for the green–blue rows the same remarks are still valid), the Fourier transform of the downsampled red signal $R_s(\omega)$ is related to the Fourier transform of the original red component $R(\omega)$ as

$$R_s(\omega)=\frac{1}{2}R(\omega)-\frac{1}{2}R(\omega-\pi). \tag{2}$$

If we interpolate R_s with a filter h_1, G_s with a filter h_0, and we add the resulting signals, as in Fig. 3(a), in the Fourier domain we have

$$\hat{G}(\omega)=\frac{1}{2}G(\omega)H_0(\omega)+\frac{1}{2}G(\omega-\pi)H_0(\omega)+\frac{1}{2}R(\omega)H_1(\omega) -\frac{1}{2}R(\omega-\pi)H_1(\omega), \tag{3}$$

where H_0 and H_1 denote the frequency responses of h_0 and h_1, respectively. Assuming high correlation between the high-frequencies of the color components, if h_1 is designed such that $H_1(\omega)\simeq 0$ at low-frequencies and $H_1(\omega)\simeq H_0(\omega)$ at high-frequencies, we have

$$R(\omega)H_1(\omega)\simeq G(\omega)H_0(\omega), \tag{4}$$

$$G(\omega-\pi)H_0(\omega)\simeq R(\omega-\pi)H_1(\omega) \tag{5}$$

and (3) can be approximated as

$$\hat{G}(\omega)\simeq\frac{1}{2}G(\omega)H_0(\omega)+\frac{1}{2}R(\omega)H_1(\omega). \tag{6}$$

A good choice for a filter h_1 that respects the constraints (4) and (5) is the five-coefficients FIR $[-0.25, 0, 0.5, 0, -0.25]$. The frequency responses of h_0 and h_1 are shown in Fig. 3(b).

This approach to estimate the green component is used by most of the edge-directed methods presented in this section and in Section 3. This technique is improved in [19], where the edge estimation is performed analyzing the variances of the color differences, and in [20], where Tsai and Song exploit the correlation between the color components to introduce a hard-decision rule and identify the best direction for the interpolation.

Another class of algorithms [21–23] proposes a weighted sum for the reconstruction of the colors. Every missing sample is estimated by its neighboring pixels and the weights are calculated on the basis of the edge directions. Some weighted sum-based techniques are considered also by Lukac et al. in [24–26] and other papers, jointly to suitable assumptions on the smoothness of the color ratios or the color differences. Instead, Chang and Chen [27] present a weighting policy based on the stochastic characteristics of uniformly oriented edge indicators, modeling the image as a 2-D locally stationary Gaussian process.

Other more complex approaches are based on different techniques such as pattern matching [28], pattern recognition [11] or the use of a threshold-based variable number of gradients measured in a neighborhood of the missing pixel [29]. Instead, Freeman [30] proposes to use the median filter to improve the reconstruction near the edges, and this approach is extended in [31] considering a vector median filtering. Another non-linear technique is presented by Ramanath et al. in [32], exploiting the bilateral filters [33].

3. Demosaicking by directional interpolations

A very interesting demosaicking strategy applies the scheme of Fig. 3(a), proposed by Hamilton and Adams, both along the horizontal and the vertical directions, producing two full color images. This leads to two estimation candidates for each pixel, and then the best of them is chosen *a posteriori* (see Fig. 4), differently from the previous approaches presenting an edge estimation followed by an edge-directed interpolation.

In [34] the decision is performed exploiting the local homogeneity of the image, as measured in the CIELab color space. For each pixel the direction of interpolation giving the most homogeneous neighborhood around the estimated pixel is chosen. Then, an iterative refining step is applied,

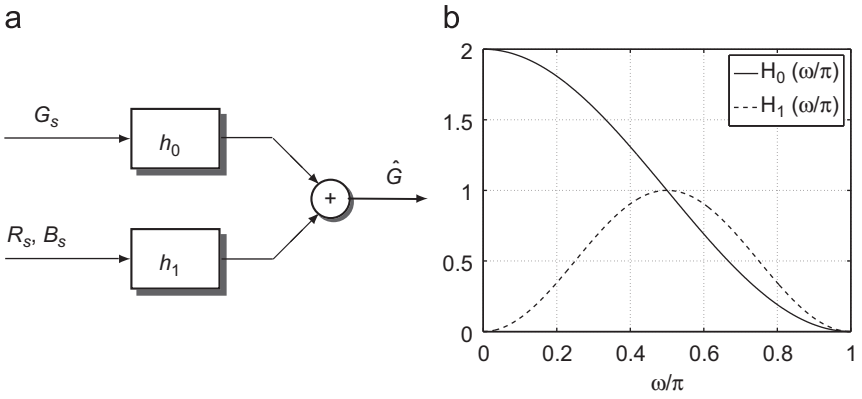

Fig. 3. (a) Reconstruction of the green signal along a row (column) with the technique of [16] and (b) Frequency response of the two filters h_0 and h_1.

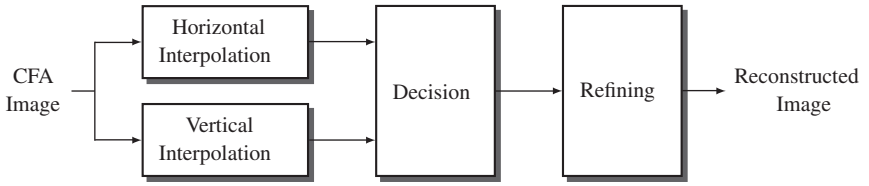

Fig. 4. Scheme of the demosaicking approaches described in Section 3.

based on a median filtering of the color differences. Instead, in [35] the decision is performed observing which directional reconstruction preserves the highest correlation of the color gradients, as usually found in natural images. While the approaches proposed in [34,35] require two interpolations of the full color image and a decision between them involving all the three color components, in [36] only the green channel is interpolated both horizontally and vertically and the decision for the best interpolation is carried out on the basis of the estimated values and of the CFA samples, producing an estimate of the green component. Then, the missing red and blue samples are reconstructed exploiting the correlation with the green ones, and an adaptive refining step is applied in order to improve the quality of the reconstructed color image.

An alternative to this procedure consists in the fusion of the horizontally and the vertically interpolated values. The reconstructed image is obtained as a weighted sum of both the estimates, and the weights are computed in order to prefer the interpolation along the direction of the edges rather than across them. This method is used in [37–39]. The weights are computed in [37] with a linear minimum mean square error estimation, while in [38] the fusion is driven by a suitable waveled-based edge estimation on the luminance component. Finally, Paliy et al. [39] use the local polynomial approximation (LPA) and the paradigm of the intersection of confidence intervals to fuse the two directional interpolations. The fusion of the directional interpolated estimates is explored also by Su and Tseng [40]. They extend the demosaicking method proposed in [36] using a similar approach for the decision of the best reconstruction in the edge points, but fusing horizontal and vertical interpolated values in the smooth regions.

In [41] the interpolation filters are obtained with the application of Taylor series and cubic spline interpolation and are applied along four opposite directions. The estimated values are filtered with a weighted median filter based on a edge orientation map in order to preserve edges.

4. Frequency domain approaches

Many demosaicking approaches are based on a frequency-domain analysis. Using the multidimensional notation described by Dubois in [42], an image acquired with a CFA over a lattice $\mathbf{\Lambda}$ is given by the sum of the three color components $X_s(\boldsymbol{n})$, for $X=R,G,B$, and $\boldsymbol{n} \in \mathbf{\Lambda}$, that are related to the full-resolution components $X(\boldsymbol{n})$ as in Fig. 5, where

- $\mathbf{\Gamma}_X$ is the sampling structure over which the color component X is acquired;

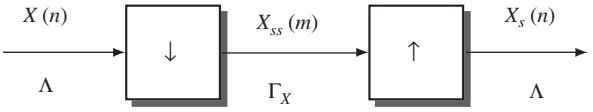

Fig. 5. Scheme of image sampling and zero-insertion interpolation.

- $X_{ss}(\boldsymbol{m})$, for $\boldsymbol{m} \in \mathbf{\Gamma}_X$, is the sampled version of X defined on the structure $\mathbf{\Gamma}_X$;
- $X_s(\boldsymbol{n})$ is the image upsampled with the zero-insertion technique.

The input–output relation between $X_s(\boldsymbol{n})$ and $X(\boldsymbol{n})$ can be expressed in the frequency domain as

$$X_s(\boldsymbol{\omega}) = \frac{1}{(\mathbf{\Lambda} : \mathbf{\Gamma}_X)} \sum_{\boldsymbol{k} \in \mathbf{\Gamma}_X^*} X(\boldsymbol{\omega} + \boldsymbol{k}), \tag{7}$$

where $(\mathbf{\Lambda} : \mathbf{\Gamma}_X)$ is the index of $\mathbf{\Gamma}_X$ in $\mathbf{\Lambda}$ and $\mathbf{\Gamma}_X^*$ the reciprocal lattice of $\mathbf{\Gamma}_X$ [42].

Therefore, denoting with ω_1 and ω_2 the horizontal and the vertical frequencies, respectively, the following relations are found for images acquired with the Bayer pattern,

$$\begin{aligned} R_s(\omega_1,\omega_2) &= \frac{1}{4}[R(\omega_1,\omega_2) - R(\omega_1-\pi,\omega_2-\pi) + R(\omega_1-\pi,\omega_2) \\ &\quad - R(\omega_1,\omega_2-\pi)], \\ G_s(\omega_1,\omega_2) &= \frac{1}{2}[G(\omega_1,\omega_2) + G(\omega_1-\pi,\omega_2-\pi)], \\ B_s(\omega_1,\omega_2) &= \frac{1}{4}[B(\omega_1,\omega_2) - B(\omega_1-\pi,\omega_2-\pi) + B(\omega_1-\pi,\omega_2) \\ &\quad - B(\omega_1,\omega_2-\pi)]. \end{aligned} \tag{8}$$

In [43] it is observed that the spectrum of the sampled green component $G_s(\omega_1,\omega_2)$ presents less aliasing replicas with respect to the sampled red and blue channels. Therefore the green component is estimated using a diamond shape 2-D filter and the red and green samples are computed using a rectangular filter. Moreover, since it is assumed that the color components share the high-frequency values, the high-frequency component of the green is used to improve the reconstruction of the red and blue channels and reduce the aliasing in the image.

Relevant considerations for the design of frequency-domain demosaicking approaches come from the work of Alleysson et al. [44]. They observed that the spectrum of an image sampled according to the Bayer pattern is given by the sum of the spectra of the three color components reported in (8). Then it can be expressed as (see Fig. 6(a))

$$\begin{aligned} \mathcal{I}_s(\omega_1,\omega_2) &= L(\omega_1,\omega_2) + C_1(\omega_1-\pi,\omega_2-\pi) + C_2(\omega_1-\pi,\omega_2) \\ &\quad - C_2(\omega_1,\omega_2-\pi), \end{aligned} \tag{9}$$

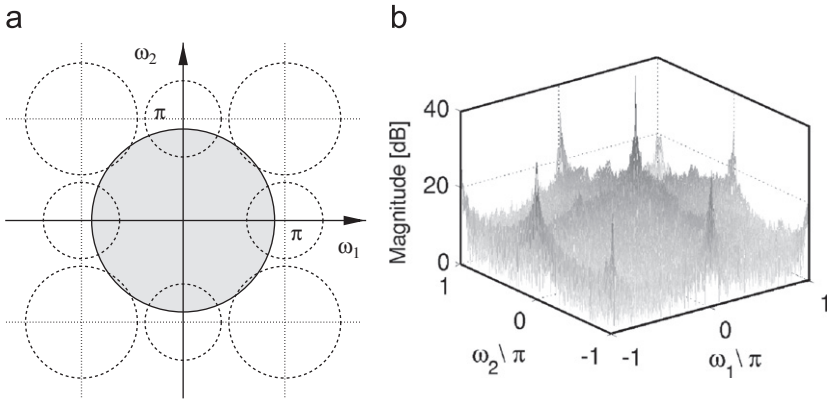

Fig. 6. (a) Support of the spectrum of a CFA image: luminance component (filled circle) and chrominance components (dotted circles) and (b) spectrum of the test image *lighthouse* after sampling with the Bayer pattern.

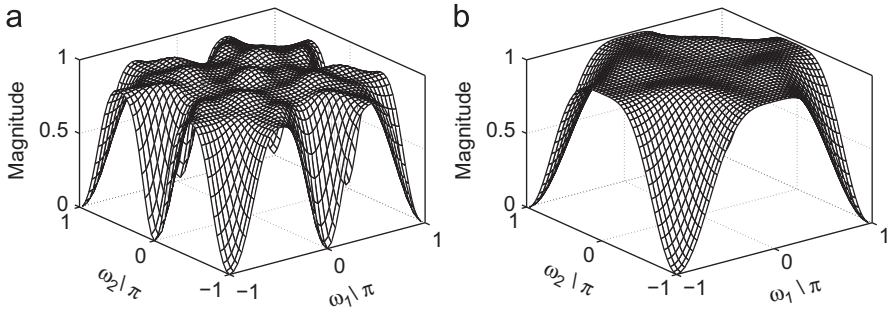

Fig. 7. (a) Frequency response of the filter to estimate the luminance proposed in [44] and (b) frequency response of the filter proposed in [45] to reconstruct the luminance in the green pixels.

where

$$L(\omega_1,\omega_2)=\frac{R(\omega_1,\omega_2)+2G(\omega_1,\omega_2)+B(\omega_1,\omega_2)}{4}, \tag{10}$$

$$C_1(\omega_1,\omega_2)=\frac{-R(\omega_1,\omega_2)+2G(\omega_1,\omega_2)-B(\omega_1,\omega_2)}{4}, \tag{11}$$

$$C_2(\omega_1,\omega_2)=\frac{-R(\omega_1,\omega_2)+B(\omega_1,\omega_2)}{4}. \tag{12}$$

$L(\omega_1,\omega_2)$ can be considered as a *luminance* component representing the achromatic visual information of the image, while $C_1(\omega_1,\omega_2)$ and $C_2(\omega_1,\omega_2)$ represent the *chrominances*. Therefore the CFA-sampled image is equivalent to the sum of the luminance component and the modulated chrominances. For instance, Fig. 6(b) shows the spectrum of the test image *lighthouse* after acquisition with the Bayer pattern. In [44] it is proposed to obtain an estimate $\hat{L}$ of the luminance with a low-pass filter removing the frequencies around $(\pm\pi,\pm\pi)$, $(0,\pm\pi)$, and $(\pm\pi,0)$ (see Fig. 7(a)), while the subsampled versions of the *opponent chromatics* $R-L$, $G-L$, and $B-L$ are estimated through suitable modulations of $\mathcal{I}_s-\hat{L}$. Finally, the bilinear interpolation is used to produce the full-resolution opponent chromatics, and the color components are reconstructed as shown in Fig. 8.

A similar strategy is exploited also in [46], where the chrominances are estimated using suitable modulations and low-pass filters, and successively the luminance component is reconstructed. Local adaptivity is included in the estimation by extracting the edge-information from the low-frequency region of the luminance. Instead, Dubois proposes to use complementary asymmetric filters to estimate the chrominances in [47] and introduces a least-square filter design to obtain an adaptive reconstruction in [48]. Once the luminance $\hat{L}$ and the chrominances $\hat{C}_1$ and $\hat{C}_2$ are estimated, the color components are computed as

$$\begin{bmatrix}\hat{R}\\ \hat{G}\\ \hat{B}\end{bmatrix}=\begin{bmatrix}1 & -1 & -2\\ 1 & 1 & 0\\ 1 & -1 & 2\end{bmatrix}\begin{bmatrix}\hat{L}\\ \hat{C}_1\\ \hat{C}_2\end{bmatrix}. \tag{13}$$

An interesting analysis is carried out in [45]. It is observed that, due to the data sampling structure of the CFA, two different states are observed in the spectrum of a Bayer sampled image. In the red and blue positions the different frequency components are modulated as in Fig. 6(a), while in the quincunx-placed green pixels the color difference terms modulated at $(0,\pm\pi)$ and $(\pm\pi,0)$ vanish. Therefore, in these pixel locations there is less spectral overlapping between the modulated chrominances and the luminance than in the former case, and the estimation of the luminance can be accomplished with a lower-order low-pass filter with respect to the filter proposed by Alleysson et al. Then, Lian et al. propose to estimate the luminance component in the green pixels with the filter whose frequency response is reported in

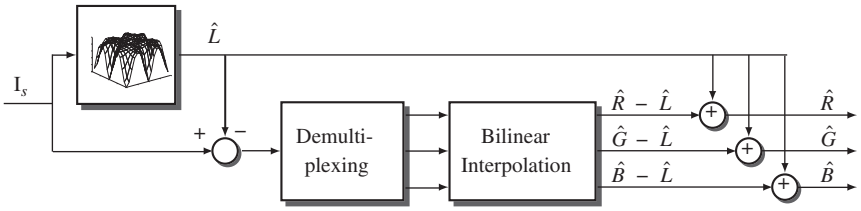

Fig. 8. Scheme of the algorithm proposed in [44].

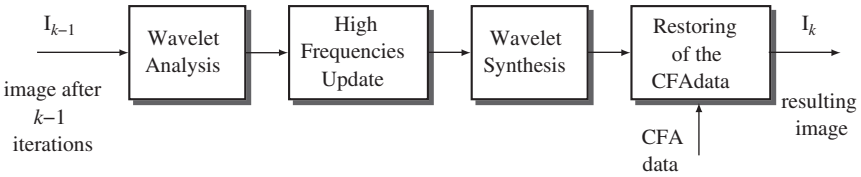

Fig. 9. Scheme of one iteration of the demosaicking method proposed in [49].

Fig. 7(b), and in the red and blue positions the luminance is computed with an adaptive strategy. After a full-resolution estimate of the luminance $\hat{L}$ is obtained, the color components are reconstructed through bilinear interpolation of $R-\hat{L}$, $G-\hat{L}$, and $B-\hat{L}$, respectively, exploiting the color values available from the CFA. Indeed, due to the correlation between the color components in the high-frequency region, the high-frequencies of the luminance are strongly correlated to the ones of the red, green and blue channels.

5. Wavelet-based methods

The correlation between the details of the different color components is exploited by some approaches in a wavelet framework. Gunturk et al. in [49] observe that, when a wavelet decomposition of the color values is performed using an appropriate wavelet basis, the high-frequency subbands of the color components are highly correlated, while the difference between the colors mainly resides in the coarsest resolution. They reconstruct the color image using the *projections onto convex sets* (POCS) technique, defining two constraints. The "observation" constraint ensures that the interpolated image is consistent with the observed data, and the "detail" constraint imposes similar high-frequency components in the color channels. These two constraint sets are shown to be convex. After an edge-directed interpolation of the three channels (using the approach in [17] or a similar technique), each of them is decomposed into four subbands and the high-frequency subbands of red and blue are updated by the projection onto the "detail" constraint (exploiting the similarity with the high-frequency subbands of the green). After the reconstruction with the synthesis filterbank, a projection onto the "observation" constraint is performed by inserting the observed data in their corresponding locations of the color components (see Fig. 9). The application of these two projections is repeated for a given number of iterations. In [50] Lu et al. provided a rigorous analysis of this approach, concluding that there is an unique fixed point that is the solution to a constrained quadratic minimization problem (see also Section 6). Basing on these considerations, they presented a method that obtains the same results of the POCS algorithm in a single step, implemented as linear filtering in the polyphase domain. A similar approach to the method of Gunturk et al. is proposed also by Li in [51], where a different analysis filterbank is used and a stopping criterion for the iterative stage is described.

In [52], after a simple demosaicking procedure, an estimate of the luminance component is obtained and its wavelet coefficients are used to correct the coefficients of the three color components. Instead, in [53] each of the three color channels reconstructed with an initial demosaicking algorithm is sampled, obtaining four polyphase components, namely X_{00}, X_{01}, X_{10}, and X_{11}, for $X=R$, G and B. Note that, with the pattern shown in Fig. 1(a), the polyphase components G_{00}, G_{11}, R_{01}, and B_{10} belong to the observed CFA image, thus their high-frequencies are not affected by interpolation errors. Successively, all the polyphase components are wavelet decomposed, and in the red positions the high-frequencies of the green and blue polyphase components are replaced with the high-frequencies of the red component. The same procedure is performed in the green and blue locations. Finally, an inverse wavelet transformation is applied to all the components and the full-resolution color channels are reconstructed.

A different approach is followed in [54], where the high frequencies of the interpolated components are refined exploiting the inter-scale correlation of the discrete wavelet transform.

Gu et al. [55] start from the frequency-domain analysis described in Section 4 to design a filterbank-based demosaicking method. Under the assumption of sparsity of the high-frequency coefficients, the reconstruction of the chrominances is reinterpreted as a robust regression scheme. Additional *a priori* knowledge about the image (for instance obtained by applying an edge-detection procedure) can be used to improve the performance of regression.

6. Reconstruction approaches

The CFA-sampled image $\mathcal{I}_s(\boldsymbol{n})$, where $\boldsymbol{n}$ represents the pixel location, can be represented as the output of the following image formation model:

$$\mathcal{I}_s(\boldsymbol{n}) = H\mathcal{I}(\boldsymbol{n}) + \eta(\boldsymbol{n}), \tag{14}$$

where $\mathcal{I}(\boldsymbol{n})$ denotes the original image, $\eta(\boldsymbol{n})$ is an additive noise introduced by the sensor (uncorrelated to $\mathcal{I}(\boldsymbol{n})$), and H is a linear operator that takes into account the image acquisition process with the CFA. Therefore, demosaicking corresponds to the inverse problem of (14), that is to find an estimate $\hat{\mathcal{I}}(\boldsymbol{n})$ of the original image $\mathcal{I}(\boldsymbol{n})$, given the observed data $\mathcal{I}_s(\boldsymbol{n})$.

One possible solution can be achieved by the *maximum a posteriori probability* (MAP) formulation, where $\mathcal{I}_s$, $\mathcal{I}$, and η are assumed random processes and the MAP estimate is given by

$$\hat{\mathcal{I}} = \underset{\mathcal{I}}{\operatorname{argmax}}\, p(\mathcal{I}|\mathcal{I}_s), \tag{15}$$

where $p(\mathcal{I}|\mathcal{I}_s)$ indicates the conditional probability density function of the random process $\mathcal{I}$ given $\mathcal{I}_s$. Using the Bayes rule, we obtain

$$\hat{\mathcal{I}} = \underset{\mathcal{I}}{\operatorname{argmax}}\, p(\mathcal{I}_s|\mathcal{I})p(\mathcal{I}). \tag{16}$$

To find $\hat{\mathcal{I}}$ using (16) the knowledge of the probability density function (PDF) $p(\mathcal{I})$ for the original image $\mathcal{I}$ is necessary. Brainard [56] assumes that the images lie in an appropriate space $\mathcal{B}$, which basis is composed by spatial sinusoids in each color bands. Therefore, the vector representation of $\mathcal{I}$ is given by

$$\boldsymbol{i} = \boldsymbol{B}\boldsymbol{w}, \tag{17}$$

where $\boldsymbol{w}$ is a multivariate gaussian process with PDF $\mathcal{N}(\boldsymbol{m}_w,\boldsymbol{K}_w)$, with $\boldsymbol{m}_w$ and $\boldsymbol{K}_w$ denoting the mean and the covariance matrix, respectively, and the columns of the matrix $\boldsymbol{B}$ are the basis of the space $\mathcal{B}$. The PDF of the image $\boldsymbol{i}$ is defined as $\mathcal{N}(\boldsymbol{B}\boldsymbol{m}_w,\boldsymbol{B}\boldsymbol{K}_w\boldsymbol{B}^T)$. Due to this formulation chosen for $\mathcal{B}$, the spectra of the natural images fall off rapidly and the different color components are positively correlated. This technique is extended in [57].

Another Bayesian approach to demosaicking is proposed in [58]. In this case the Markov random fields (MRF) model is considered for the *a priori* probability $p(\mathcal{I})$ and a simulated annealing technique is applied. The MRF model is proposed also in [59] to describe both the luminance and the chrominances components, and the solution is found using POCS or the steepest descent technique. In [60] the steerable wavelets are used to decompose the image into a set of oriented subbands whose coefficients have Laplacian distribution. Therefore, the *a priori* model for the image is given by the sum of the Laplacian PDF of any subband.

An alternative formulation to find a solution to the inverse problem of (14) is given by the *minimum mean-squared error* (MMSE) method. In this case, the best linear estimate $\hat{\mathcal{I}}$ is obtained minimizing the average mean square error

$$E[\|\mathcal{I}-\hat{\mathcal{I}}\|^2]. \tag{18}$$

This leads to the following solution:

$$\hat{\mathcal{I}} = r_{\mathcal{I}\mathcal{I}_s}(r_{\mathcal{I}\mathcal{I}})^{-1}\mathcal{I}_s, \tag{19}$$

where $r_{\mathcal{I}\mathcal{I}_s}$ denotes the correlation function between $\mathcal{I}$ and $\mathcal{I}_s$, and $r_{\mathcal{I}\mathcal{I}}$ the autocorrelation of $\mathcal{I}$. For gaussian distributions the MAP and MMSE estimates are identical.

A demosaicking technique based on a MMSE approach is proposed in [61] with a frequency-domain analysis and a scale-invariant prior for the original image, that is assumed to have the following power spectral density:

$$\mathcal{P}_{\mathcal{I}}(\omega_r,\omega_\theta) = \mathcal{F}_{\omega_r,\omega_\theta}(E[\mathcal{I}\mathcal{I}^*]) = \frac{1}{\omega_r^2} f(\omega_\theta)\Gamma_0, \tag{20}$$

where ω_r and ω_θ are the radial and angular frequencies, respectively. The angular distribution $f(\omega_\theta)$ is usually taken as constant, and Γ_0 is another constant arising from surface spectral reflectances. This image prior is used to derive an optimal constrained MMSE estimator. A proof for the existence of the constrained solution to (18) is also given, providing key insight required for the construction of the linear operator.

A MMSE approach is considered also in [62], where Trussell and Hartwig exploit simple assumptions on color images to propose a cost-effective method reducing the dimensions of the huge matrices and allowing fast implementations. Instead, Portilla et al. in [63] introduce a joint spatial-chromatic correlation model trained on a small set of images. A similar idea to obtain the prior model for the color images is presented also in [64].

An alternative to find a solution to the inverse problem of (14) is given by the regularization methods. As for the statistical approaches, the role of regularization is to exploit the *a priori* knowledge about natural images, in order to convert an ill-posed problem into a well-posed one [65,66]. Regularization is widely used in many aspects of reconstruction and restoration of digital images, such as denoising, deblurring, motion estimation, magnification or super-resolution.

The *regularized solution* $\hat{\mathcal{I}}$ is defined as the solution of the following problem:

$$\hat{\mathcal{I}} = \underset{\mathcal{I}}{\operatorname{argmin}}\left\{ \Psi(\mathcal{I},\mathcal{I}_s) + \sum_k \lambda_k J_k(\mathcal{I}) \right\}, \tag{21}$$

where the first term $\Psi(\mathcal{I},\mathcal{I}_s)$, called *data-fidelity term*, denotes a measure of the distance between the estimated image and the observed data, while the terms $J_k(\mathcal{I})$ are some regularizing constraints based on a *a priori* knowledge of the original image. The regularization parameters λ_k control the tradeoff between the different terms.

Keren and Osadchy propose a regularization approach to demosaicking in [67], exploiting two regularizing constraints. The first one is composed by the first-order derivatives in the horizontal, vertical and diagonal directions, respectively, and is used to impose smoothness on each color component. The second constraint is given by the sum of the outer product of each pixel vector $[R(\boldsymbol{n}),G(\boldsymbol{n}),B(\boldsymbol{n})]$ with the vectors representing its neighboring pixels. In this way the regularization forces also the color components to be correlated. This technique is considered also in the joint demosaicking and super-resolution approach presented in [68] that will be analyzed

in Section 8. Another regularization method to demosaicking is proposed in [69], using the total-variation criterion to impose smoothness both on the single color components and on the color differences. An iterative algorithm to find the solution of (21) is presented also in [70]. Omer and Tanaka [71] introduce a novel regulating term to impose smoothness on the chrominances and use suitable edge-directed weights to avoid over-smoothing across the edges. In [72,73] the regularization is imposed first using quadratic constraints, then with a novel approach to make adaptive the reconstruction method. Moreover, it is shown that the regularization techniques can handle effectively also non-ideal acquisition devices.

Another competitive demosaicking algorithm is proposed in [74], exploiting the optimal recovery estimation theory. It estimates the missing pixels of some local image patches from the known pixels, under the assumption that each local patch belongs to a known quadratic signal class. The optimal recovery estimate for the missing value minimizes the maximum error over all possible vectors belonging to the signal class that have the same known samples.

The sparse nature of the color image is exploited also in [75], where a demosaicking approach is proposed in the spirit of the compressed sensing theory. Natural images are assumed to admit a sparse decomposition over a redundant dictionary. Therefore, a well-adapted dictionary is designed and learned with an iterative method that incorporates the K-SVD (single value decomposition) algorithm, in order to be used for the reconstruction of the CFA-sampled images. In [76] the ℓ_1 norm is adopted to design the data-fidelity term and the constraint on the color differences and a *principal component analysis* (PCA) is used to describe the sparse nature of single color components. Then the solution of the minimization problem is estimated with an iterative algorithm. Another reconstruction method is proposed by Buadeset al. in [77] taking into account the non-local image geometry, while in [78] an energy functional is defined and its minimization, through a level set procedure, gives the edge-direction to drive the image reconstruction.

Almost all described demosaicking methods are based on the assumption of high correlation between the color components. Zhang et al. in [79] analyze some techniques to reconstruct the color image when this assumption is not fulfilled. They describe an optimal fusion problem to combine existing demosaicking approaches with an adaptive intraband interpolation and propose two solutions, one based on linear minimum mean square estimation and the other making use of the support vector regression.

7. Joint demosaicking and zooming

Many digital devices, after the demosaicking procedure, need a zooming of the image to increase the resolution. Many techniques to image interpolation have been proposed (see for instance [80,81]), and usually zooming and demosaicking are considered separately. However, this solution presents some relevant drawbacks:

- the computational cost is high due to the application of both demosaicking and zooming. Moreover the zooming algorithm has to be applied to each color component;
- the color artifacts introduced by the demosaicking reconstruction are expanded by the zooming;
- some image interpolation techniques are adaptive, and the detection of the edges can be affected by the demosaicking artifacts, especially in correspondence of details.

Therefore, in literature, some joint demosaicking and zooming approaches are considered. In this way, the raw data are processed according to the desired resolution, only one edge-detection analysis is performed instead of applying it both in the demosaicking and in the zooming algorithm, and the analogies between these two interpolation procedures are exploited. Moreover, the computational cost is kept lower with respect to the application of demosaicking and zooming independently.

Recently two approaches to the joint demosaicking and zooming problem have been proposed in [82,83]. Both techniques start with the reconstruction of the green component and produce an estimate of this component at the same resolution of the CFA image, exploiting two directional interpolation and a decision for the best reconstruction, as explained in Section 3. Then, the green component is magnified at the desired resolution and is used to drive the interpolation of the red and blue channels exploiting the correlation between the color values. Both the approaches give better performances with respect to apply demosaicking and zooming separately.

Another method to increase the resolution starting from the raw data is proposed in [84,85]. In this case, an estimation of the CFA-sampled image at the desired resolution is performed, then classical demosaicking approaches can be applied.

8. Joint demosaicking and super-resolution

Another approach to enhance the spatial resolution is to fuse several low-resolution images of the same scene, in order to produce a high-resolution image (or a sequence of them). It is called *super-resolution* and is proved to be useful in many practical situations where multiple frames of the same scene are available, including medical imaging, satellite imaging, videosurveillance and other video applications. Many techniques to super-resolution have been proposed and an overview of them can be found in [86]. Since the low-resolution images are often acquired by digital cameras provided with a CFA, it is interesting to perform super-resolution from the raw data directly, that is to consider demosaicking and super-resolution jointly.

A solution to this problem is proposed in [68] with a regularization method that exploits several regularizing constraints. One of them imposes smoothness to the luminance component with the bilateral total-variation technique, an extension of the total-variation criterion [87] in the spirit of the bilateral filters [33]. A quadratic penalty term is used to describe the bandlimited characteristic of the chrominances, and another term penalizes the mismatch between locations or orientation of edges across the color bands, generalizing the vector product-based term

introduced in [67]. The data-fidelity term measuring the similarity between the resulting high-resolution image and the original low-resolution images is based on the ℓ_1 norm. A steepest descent optimization is applied to minimize the cost function. Another regularization approach to joint demosaicking and super-resolution is described in [88], using the Tikhonov method of regularization.

A different strategy is followed in [89]. The luminance and the chrominances components are extracted from the CFA image according to the approach of Alleysson et al. described in Section 4, then are interpolated to obtain their high-resolution versions. Finally, the high-resolution color image is reconstructed.

9. Joint demosaicking and denoising

The acquisition of an image introduces a noisy component due to the photon counting process and the electrical and thermal effects in the sensor. Therefore, a digital camera pipeline has to consider also a *denoising* procedure to remove the noise from the acquired image. In literature, many denoising approaches have been proposed, exploiting, for instance, the Wiener filtering, the total-variation regularization [87] or the bilateral filters [33]. Most of the denoising approaches apply linear transformations that are able to separate low and high-frequencies (such as the wavelets, the curvelets or the contourlets). In fact, it is observed that natural images concentrate the energy in the lowest frequencies, while in the high-frequency subbands the energy is localized only in correspondence of the details of the image. On the other hand, if the noise is assumed white, its distribution is constant over all the spectrum. Therefore, many denoising approaches [90–93] apply a linear transformation (such as the wavelets), then "clean" the high-frequency subbands simply thresholding them. Finally, an inverse transformation of the "cleaned" coefficients is performed to obtain the denoised image. This procedure is based on the idea that large coefficients, which are kept, belong to the details of the image, whereas the noise is distributed across small coefficients, which are canceled.

Denoising can be performed before demosaicking [94,95], or after the color reconstruction. However, both the solutions present relevant drawbacks. In the first case denoising has to be accomplished considering separately the three color components, and it does not allow for analyzing the image at the maximum resolution, which is important to exploit the frequency sparsity of the natural images. Otherwise an *ad hoc* approach for the CFA has to be considered, such as in [95] where a principal component analysis is performed. On the other hand, if demosaicking is performed before denoising, it is applied on a noisy image, making difficult the edge estimation that is an important task of the adaptive approaches. Moreover, the demosaicking procedure modifies the statistical characteristics of the noise, and it complicates the application of the denoising approaches that are based on particular assumptions about the noise. It has to be pointed out also that to denoise color images require to remove the noise on all the three color components, thus increasing the computational cost.

Therefore a more efficient solution is to consider denoising and demosaicking jointly. This approach is proposed in [96] using the total least square denoising to remove both signal-independent and signal-dependent noises. Another technique is described in [97] using a Bayesian hierarchical modeling to capture the second-order statistics in the wavelet domain. An EM (expectation-minimization) algorithm is coupled with the Bayesian model, in order to obtain the reconstruction of the unobserved data and the denoising of the whole image starting from the available data. Instead, in [98] a wavelet transform of the noisy CFA-image is performed, and the wavelet coefficients of the luminance and the chrominances components are estimated and denoised. Finally, an inverse wavelet transform is applied and the color image is reconstructed.

Zhang et al. in [99] recover the green component by estimating the color differences with a MMSE approach that exploits both spectral and spatial correlations to simultaneously suppress sensor noise and interpolation error. Then, the CFA channel-dependent noise is removed from the reconstructed green channel with a wavelet-based approach. Finally, also the red and blue channels are estimated and denoised. Instead the method in [100] is based on the local polynomial approximation (LPA) and the paradigm of the intersection of confidence intervals to design and choose suitable filters to denoise and interpolate the CFA samples.

In [101] an evaluation of the statistical characteristics of the noise after demosaicking of a noisy image with the space-varying filters designed in [73] is reported, and is extended in order to propose a strategy remove the noise from the demosaicked image.

Condat [102] proposes a strategy for joint demosaicking and denoising by extending the frequency-domain demosaicking approach proposed by Dubois in [47,48] previously described in Section 4. Wiener filters are designed to obtain a denoised version of the chrominances, while the luminance is denoised as a grayscale image corrupted by white noise. Finally, the color components are computed as in (13).

10. Quality assessment of demosaicking approaches

In literature, a commonly used approach for evaluating demosaicking algorithms consists of choosing some full-resolution color images, sampling them according to the Bayer pattern (or other CFA arrangements), applying the demosaicking procedure to the sampled images, and comparing the results with the original images. Lower is the difference between the original images and their respective reconstructed versions, better is the effectiveness of the algorithm. As a measure of the difference, usually the *mean square error* (MSE) is considered, that is given, for each color component $X(n_1,n_2)$, with $X=R,G,B$, and $n_1=1,\ldots,N_1$, $n_2=1,\ldots,N_2$, by

$$\mathrm{MSE}(X)=\frac{1}{N_1N_2}\sum_{n_1=1}^{N_1}\sum_{n_2=1}^{N_2}(\hat{X}(n_1,n_2)-X(n_1,n_2))^2. \tag{22}$$

Alternatively a logarithmic measure is preferred, such as the *peak signal-to-noise ratio* (PSNR) or the *color peak signal-to-noise ratio* (CPSNR), defined as [44]

$$\mathrm{CPSNR} = 10\log_{10}\frac{255^2}{\frac{1}{3}\sum_{X=R,G,B}\mathrm{MSE}(X)}. \quad (23)$$

However, it is found that the MSE is not representative enough of the difference between two images, as perceived by human observers. In order to give an evaluation closer to the human visual perception than the CPSNR measure, often the S-CIELAB metric [103] is used to quantify the performance of the different demosaicking algorithms. S-CIELAB measures how accurate the reproduction of a color is to the original when viewed by a human observer. It is an extension of the CIE$L^*a^*b^*$ ΔE color difference formula exploiting also a spatial pre-processing step that incorporates the pattern-color sensitivity measurements proposed by Poirson and Wandell [104,105] in order to simulate the spatial blurring by the human visual system. The reproduction error is measured as the difference between the S-CIELAB representation of an original image and its reconstructed version.

Moreover, often these numerical considerations are combined with a visual inspection of some detailed regions where many demosaicking methods typically fail. Test-images are commonly taken from the Kodak dataset that are available in [106] (see Fig. 10). These images are film captured and then digitized at the resolution of 512×768 pixels with 8 bit depth per component. In this dataset there are a lot of details that allow for an immediate evaluation of the quality of the demosaicking procedures. However, despite its popularity in literature, the film captured images of the Kodak dataset are not

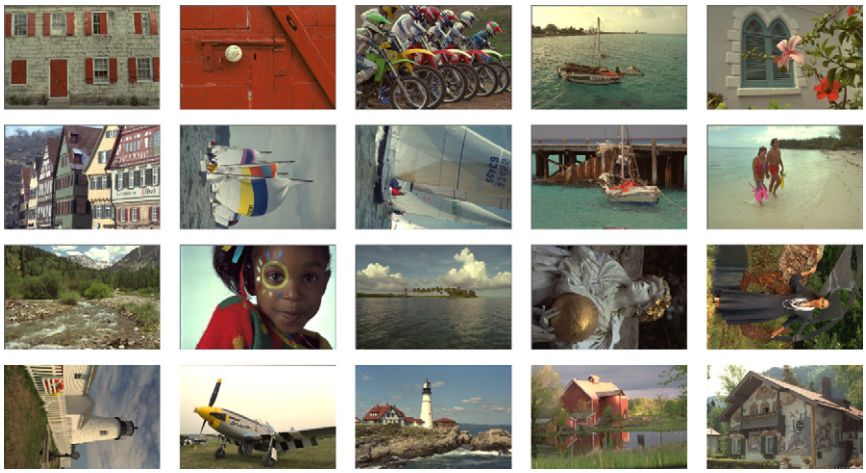

Fig. 10. The test images of the Kodak dataset.

Table 1
CPSNR (dB) results for different demosaicking methods.

Method	[19]	[20]	[34]	[37]	[38]	[44]	[45]	[47]	[49]	[51]	[73]	[75]
1	38.58	36.59	35.15	38.36	39.15	36.18	37.58	38.08	37.90	38.44	38.04	**39.32**
2	40.18	40.30	38.88	40.42	38.31	36.16	40.26	38.80	38.54	35.51	38.16	**40.66**
3	38.08	37.55	35.48	38.05	38.03	35.62	38.12	37.92	37.23	35.08	38.17	**38.67**
4	40.10	38.71	37.59	40.03	**40.41**	37.08	38.11	39.97	38.68	39.14	39.66	39.98
5	42.15	42.37	40.33	42.03	41.80	38.89	42.69	41.89	41.21	39.11	42.39	**42.70**
6	36.50	35.22	33.83	35.96	**36.76**	32.52	35.37	35.32	35.56	35.66	36.01	36.39
7	**43.11**	42.22	40.96	42.76	42.98	39.37	42.72	42.24	41.71	41.46	42.38	43.03
8	42.60	41.37	40.56	41.77	42.46	39.67	**42.69**	42.18	41.06	40.90	42.46	42.64
9	40.07	39.15	37.59	40.10	**40.25**	37.47	39.47	39.84	39.34	38.91	39.78	40.16
10	**43.54**	42.42	41.57	42.81	43.43	39.24	42.77	42.92	41.86	41.65	43.07	43.38
11	35.03	32.83	31.45	34.73	35.58	34.52	33.89	35.18	34.46	**35.71**	34.62	35.27
12	39.61	38.87	37.72	39.17	38.72	36.54	39.53	39.18	38.40	37.25	39.18	**40.14**
13	43.87	42.10	41.49	43.26	**44.18**	39.82	41.30	43.75	41.84	42.14	43.28	43.47
14	41.74	40.57	39.31	41.43	41.73	39.95	41.58	41.77	40.93	41.12	41.59	**41.84**
15	36.97	35.77	34.12	36.48	37.12	35.63	36.76	36.85	36.50	36.21	37.01	**37.47**
16	40.65	39.79	38.04	40.46	41.09	36.51	40.01	40.16	39.80	40.16	39.97	**41.14**
17	**41.06**	37.54	38.55	37.80	40.69	38.23	40.54	39.94	37.48	39.19	40.63	40.86
18	39.37	37.84	36.50	38.93	39.61	37.25	38.70	38.81	38.67	39.13	39.16	**39.69**
19	38.38	38.45	36.35	38.55	38.16	36.50	38.64	38.00	37.73	37.17	38.47	**38.83**
20	35.07	34.16	32.79	34.91	34.76	34.36	34.64	35.13	34.14	34.54	35.30	**35.59**
Ave.	39.83	38.69	37.41	39.40	39.76	37.08	39.27	39.40	38.65	38.42	39.47	**40.06**

Table 2
S-CIELAB results for different demosaicking methods.

Method	[19]	[20]	[34]	[37]	[38]	[44]	[45]	[47]	[49]	[51]	[73]	[75]
1	1.104	1.204	1.238	1.117	**1.053**	1.507	1.205	1.167	1.279	1.271	1.205	1.064
2	0.707	0.727	0.829	0.696	0.886	1.142	0.694	0.778	0.806	1.136	0.929	**0.683**
3	1.018	1.048	1.278	1.079	1.090	1.404	1.004	1.041	1.240	1.687	1.112	**0.968**
4	0.802	0.847	0.864	0.817	**0.786**	1.147	0.955	0.788	1.012	1.009	0.872	0.872
5	0.594	0.559	0.689	0.595	0.638	0.915	**0.536**	0.559	0.689	0.935	0.606	0.567
6	**1.252**	1.358	1.415	1.341	1.294	1.958	1.381	1.458	1.564	1.643	1.387	1.409
7	**0.556**	0.577	0.633	0.572	0.572	0.818	0.571	0.580	0.674	0.699	0.638	0.576
8	0.544	0.572	0.612	0.558	0.557	0.756	**0.535**	0.550	0.637	0.674	0.605	0.549
9	0.742	0.754	0.838	0.734	**0.733**	1.037	0.787	0.748	0.850	0.919	0.793	0.791
10	**0.473**	0.511	0.523	0.496	0.499	0.756	0.509	0.476	0.595	0.624	0.537	0.520
11	1.567	1.753	1.868	1.553	**1.492**	1.659	1.661	1.557	1.805	1.723	1.604	1.551
12	0.682	0.736	0.809	0.724	0.788	0.959	**0.674**	0.696	0.817	0.920	0.744	0.681
13	0.542	0.599	0.576	0.563	0.532	0.850	0.684	**0.527**	0.703	0.699	0.588	0.605
14	0.534	0.598	0.590	0.558	0.548	0.700	0.530	**0.513**	0.633	0.613	0.551	0.533
15	1.087	1.117	1.378	1.084	1.129	1.297	1.058	1.105	1.167	1.381	1.094	**1.001**
16	0.761	0.777	0.894	0.766	**0.746**	1.116	0.782	0.810	0.863	0.885	0.853	0.767
17	**0.576**	0.640	0.680	0.625	0.667	0.714	**0.576**	0.646	0.732	0.717	0.629	0.588
18	0.892	0.940	1.027	0.907	0.897	1.106	0.929	0.938	1.005	1.002	0.939	**0.884**
19	0.989	0.934	1.207	0.944	1.019	1.216	0.922	0.957	1.067	1.222	0.972	**0.895**
20	1.088	1.117	1.366	1.079	1.171	1.225	1.058	1.084	1.250	1.372	1.110	**1.037**
Ave.	**0.825**	0.868	0.966	0.840	0.855	1.114	0.852	0.849	0.969	1.056	0.888	0.827

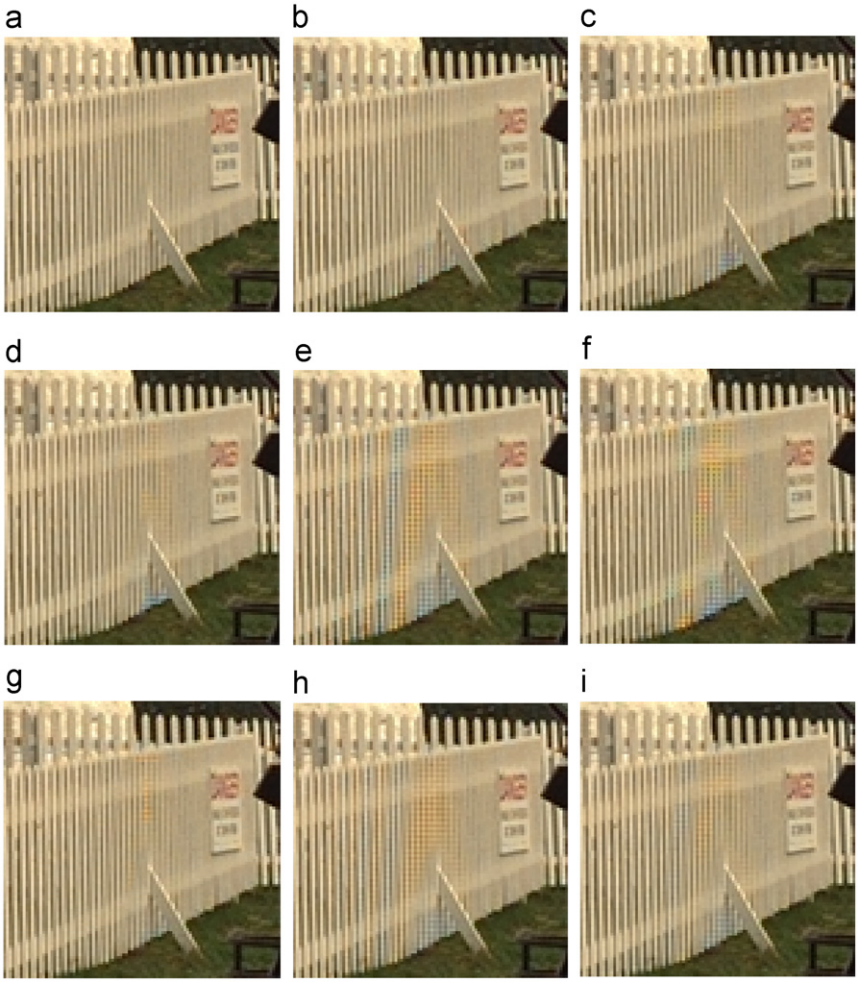

Fig. 11. (a) Portion of the test image no. 16; (b)–(i) image reconstructed using the demosaicking methods proposed in [19,37,38,45,47,49,73,75], respectively.

very representative of the data acquired by the most recent digital cameras [9]. Therefore, often it is more meaningful to test the demosaicking approaches using raw data captured using real digital cameras. In this case, however, knowledge about the "original" full-resolution image is not available, then it is not possible to measure the quality with quantitative metrics such as MSE, CPSNR or S-CIELAB. A study about a perceptual assessment of the quality of some demosaicking algorithms is reported in [57]. In the following we will provide some comparisons between the various techniques presented in literature considering both numerical evaluations over the Kodak dataset and visual inspections with raw images captured with digital cameras.

11. Comparison

To evaluate the performances of the presented demosaicking techniques we start by analyzing the CPSNR and the S-CIELAB results obtained over the test images belonging to the Kodak dataset shown in Fig. 10. Table 1 reports the CPSNR values given by the methods proposed by Chung and Chan [19], Tsai and Song [20], Hirakawa and Parks [34], Zhang and Wu [37], Menon and Calvagno [38], Alleysson et al. [44], Lian et al. [45], Dubois [47], Gunturk et al. [49], Li [51], Menon and Calvagno [73], Mairal et al. [75]. The original MATLAB code or the software provided by the authors is used for any algorithm. Boldface numbers indicates the highest values obtained for each image. The best average performances are achieved by the approach proposed by Mairal et al. that obtains also the highest CPSNR values on 11 test images, confirming the soundness of this reconstruction approach. Good performances are achieved also with the regularization method presented in [73] and with the directional approaches proposed in [19,37,38]. In particular, these techniques allow to provide simultaneously good results and reduced computational costs, thus candidate themselves for implementation in simple low-cost cameras.

It could be interesting to analyze the performances of the different methods also using the S-CIELAB metric. As reported in Table 2 (where the boldface numbers indicate the lowest S-CIELAB difference for each test image), in this case the best average result is provided by the techniques proposed in [19,75] but also the approaches of [20,37,38,47,45] obtain low S-CIELAB values.

Fig. 11 shows a portion of the original test image no. 16, and of the reconstructed versions obtained with the methods proposed in [19,37,38,45,47,49,73,75]. The estimation becomes more difficult where the fence pickets are closer, i.e., where the amount of the spatial high-frequencies increases. The best reconstruction is provided by the technique proposed in [19], but also the methods presented in [37,38,47] avoid the introduction of unpleasant false colors. In this case the edges are largely vertical, therefore the algorithms based on horizontal and vertical interpolations obtain the best results. A different behavior can be observed in Fig. 12 that shows a portion of the test image no. 6. Here the letters in the wall present a lot of details that make difficult the estimation from the CFA samples. In this case, the best performances are achieved

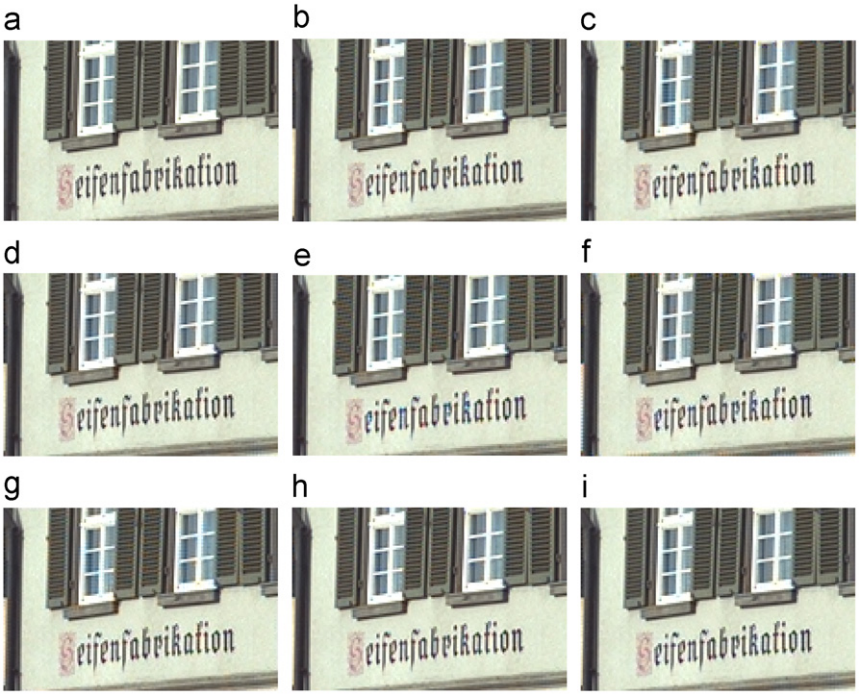

Fig. 12. (a) Portion of the test image no. 6; (b)–(i) image reconstructed using the demosaicking methods proposed in [19,37,38,45,47,49,73,75], respectively.

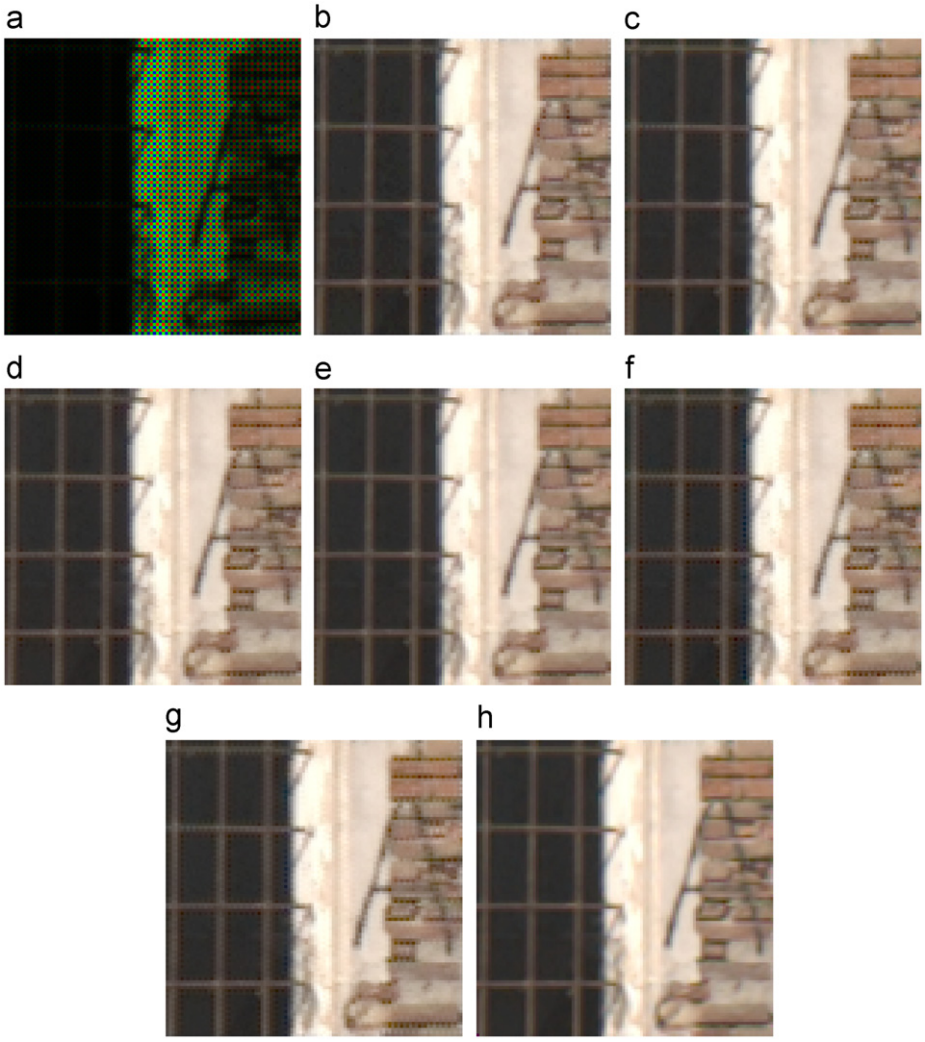

Fig. 13. Portion of an image captured using a Pentax *ist DS2 camera: (a) CFA image; (b)–(h) image reconstructed using the demosaicking methods proposed in [19,37,38,45,47,49,73], respectively.

by the reconstruction approaches proposed in [73,75], but also the methods of [19,38] provide good performances.

As stated in Section 10, it is interesting to test the demosaicking algorithms also on data acquired by real digital cameras, since often they present different characteristics with respect to the Kodak test images. Fig. 13(a) shows a 100×100 portion of an image captured using a Pentax *ist DS2 camera, which has a 6.1 megapixels CCD sensor with the Bayer pattern as CFA arrangement, and the results of the color demosaicking reconstruction using the methods presented in [19,37,38,45,47,49,73] are shown in Figs. 13(b)–(h)[1]. Most of the reconstructed images present a large amount of zipper effect. This is due to the assumption of high correlation between the color components that is the basis of each demosaicking strategy. In the case of real images this correlation is weaker, then this assumption can lead to a wrong estimation. The method proposed in [73] allows to set some regularization parameters according to the characteristics of the image that has to be reconstructed. Therefore, with a suitable adjustment of these parameters it can obtain good performances also with real data, as shown in Fig. 13(h) where the resulting image does not present zipper effect. Besides the approach of [73], good results are obtained also using the frequency-domain method described in [45].

12. Conclusion

In this paper we described several techniques proposed to demosaick the samples acquired by a digital camera provided with a color filter array and the performances of some of them are compared in the experimental section. This research problem has been analyzed by many authors and the first demosaicking techniques proposed in many patents have been improved by a lot of

[1] In this case we do not test the algorithm of [75], since the code provided us by the authors is optimized on the Kodak dataset.

research papers, allowing to obtain very high performances. In particular, good results are provided from directional approaches such as [19,37,38] and others that can be implemented with a reduced computational cost. However, it has to be considered that the images acquired from real cameras present different characteristics with respect to the standard test images, and often demosaicking solutions that perform well with the Kodak dataset do not achieve good estimation with real CFA data. Moreover, many demosaicking approaches do not consider other aspects of the image acquisition process in a digital camera, such as the point spread functions (PSF) of the imaging system or the noise introduced from the sensor that can affect the color reconstruction. For instance, the characteristics of the impulse responses of the sensors determine the spectral overlaps and the correlations of the color components in the sampled image, and the noise makes difficult the estimation of the edges. Under this perspective, the reconstruction approaches can take into account also these aspects of the acquisition process and provide efficient solutions for real CFA data, as showed in the case of Fig. 13. On the other hand, often the demosaicking methods designed with this strategy present a computational complexity that makes prohibitive an efficient implementation.

Particular attention has to be paid also to the strategies to analyze demosaicking jointly with zooming, denoising or super-resolution, as described in Sections 7–9. These approaches allow to find solutions that are more competitive with respect to consider each problem separately.

Recently, we observed novel trends in the design of the CFA arrangements. While for about 30 years since the introduction of the Bayer pattern in 1976, this scheme has been extensively used (sometimes with slight modifications, as described in Section 1) and a lot of efforts have been done to find efficient solution to demosaicking, in recent papers novel arrangements are proposed in order to allow simpler demosaicking strategies. The first results with the test images seem promising, however a lot of work has to be done to analyze the performances with real digital cameras.

Acknowledgements

The authors would thank King-Hong Chung, Chi-Yi Tsai, Keigo Hirakawa, Lei Zhang, Eric Dubois, David Alleysson, Nai-Xiang Lian, Bahadir Gunturk, and Julien Mairal for providing the code of their algorithms.

References

[1] K. Hirakawa, P.J. Wolfe, Advancing the digital camera pipeline for mobile multimedia: key challenges from a signal processing perspective, in: Proceedings of the IEEE International Conference on Acoustics, Speech and Signal Processing2008, pp. 5332–5335.
[2] P.M. Hubel, J. Liu, R.J. Guttosch, Spatial frequency response of color image sensors: Bayer color filters and Foveon X3, Technical report, Foveon, San Antonio, USA, 2002.
[3] B.E. Bayer, Color imaging array, U.S. Patent No. 3 971 065, July 1976.
[4] R. Lukac, K.N. Plataniotis, Color filter arrays: design and performance analysis, IEEE Trans. Consum. Electron. 51 (4) (2005) 1260–1267.
[5] J.F. Hamilton, J.T. Compton, Processing color and panchromatic pixels, U.S. Patent No. 2007 0024879, February 2007.
[6] K. Hirakawa, P.J. Wolfe, Spatio-spectral color filter array design for optimal image recovery, IEEE Trans. Image Process. 17 (10) (2008) 1876–1890.
[7] Y.M. Lu, M. Vetterli, Optimal color filter array design: quantitative conditions and an efficient search procedure, Proceedings of the SPIE Electronic Imaging: Digital Photography V, vol. 7250, 2009.
[8] B.K. Gunturk, J. Glotzbach, Y. Altunbasak, R.W. Schafer, R.M. Mersereau, Demosaicking: color filter array interpolation, IEEE Signal Process. Mag. 22 (1) (2005) 44–54.
[9] X. Li, B.K. Gunturk, L. Zhang, Image demosaicing: a systematic survey, Proceedings of the SPIE-IS&T Electronic Imaging, Visual Communications and Image Processing, vol. 6822, 2008.
[10] S. Battiato, M. Guarnera, G. Messina, V. Tomaselli, Recent patents on color demosaicing, Recent Pat. Comput. Sci. 1 (3) (2008) 94–207.
[11] D.R. Cok, Signal processing method and apparatus for producing interpolated chrominance values in a sampled color image signal, U.S. Patent No. 4 642 678, February 1987.
[12] J.E. Adams, Interactions between color plane interpolation and other image processing functions in electronic photography, Proceedings of SPIE, vol. 2416, 1995, pp. 144–151.
[13] R.H. Hibbard, Apparatus and method for adaptively interpolating a full color image utilizing chrominance gradients, U.S. Patent No. 5 382 976, January 1995.
[14] C.A. Laroche, M.A. Prescott, Apparatus and method for adaptively interpolating a full color image utilizing chrominance gradients, U.S. Patent No. 5 373 322, December 1994.
[15] J.E. Adams, Design of practical color filter array interpolation algorithms for digital cameras, Proceedings of SPIE, vol. 3028, 1997, pp. 117–125.
[16] J.E. Adams, Design of practical color filter array interpolation algorithms for digital cameras, part 2, Proceedings of the IEEE International Conference on Image Processing, vol. 1, 1998, pp. 488–492.
[17] J.F. Hamilton, J. Adams, Adaptive color plane interpolation in single sensor color electronic camera, U.S. Patent No. 5 629 734, May 1997.
[18] R. Kakarala, Z. Baharav, Adaptive demosaicing with the principal vector method, IEEE Trans. Consum. Electron. 48 (4) (2002) 932–937.
[19] K.-H. Chung, Y.-H. Chan, Color demosaicing using variance of color differences, IEEE Trans. Image Process. 15 (10) (2006) 2944–2955.
[20] C.-Y. Tsai, K.-T. Song, Heterogeneity-projection hard-decision color interpolation using spectral-spatial correlation, IEEE Trans. Image Process. 16 (1) (2007) 78–91.
[21] R. Kimmel, Demosaicing: image reconstruction from ccd samples, IEEE Trans. Image Process. 8 (9) (1999) 1221–1228.
[22] W. Lu, Y.-P. Tan, Color filter array demosaicing: new method and performance measures for color filter array, IEEE Trans. Image Process. 12 (10) (2003) 1194–1210.
[23] S.-C. Pei, I.-K. Tam, Effective color interpolation in CCD color filter arrays using signal correlation, IEEE Trans. Circuits Syst. Video Technol. 13 (6) (2003) 503–513.
[24] R. Lukac, K.N. Plataniotis, Universal demosaicking for imaging pipelines with an RGB color filter array, Pattern Recognition 38 (11) (2005) 2208–2212.
[25] R. Lukac, K.N. Plataniotis, D. Hatzinakos, M. Aleksic, A novel cost effective demosaicing approach, IEEE Trans. Consum. Electron. 50 (1) (2004) 256–261.
[26] R. Lukac, K.N. Plataniotis, D. Hatzinakos, M. Aleksic, A new CFA interpolation framework, Signal Process. 86 (7) (2006) 1559–1579.
[27] H.-A. Chang, H.H. Chen, Stochastic color interpolation for digital cameras, IEEE Trans. Circuits Syst. Video Technol. 17 (8) (2007) 964–973.
[28] X. Wu, W.K. Choi, P. Bao, Color restoration from digital camera data by pattern matching, Proceedings of SPIE, vol. 3018, 1997, pp. 12–17.
[29] E. Chang, S. Cheung, D.Y. Pan, Color filter array recovery using a threshold-based variable number of gradients, Proceedings of SPIE, vol. 3650, 1999, pp. 36–43.
[30] W.T. Freeman, Method and apparatus for reconstructing missing color samples, U.S. Patent No. 4 774 565, September 1988.
[31] M.R. Gupta, T. Chen, Vector color filter array demosaicing, Proceedings of the SPIE Conference on Sensors and Camera Systems for Scientific, Industrial, and Digital Photography Applications II, vol. 4306, 2001, pp. 374–382.
[32] R. Ramanath, W.E. Snyder, Adaptive demosaicking, J. Electron. Imaging 12 (4) (2003) 633–642.

[33] C. Tomasi, R. Manduchi, Bilateral filtering for gray and color images, in: Proceedings of the IEEE International Conference on Computer Vision1998, pp. 839–846.
[34] K. Hirakawa, T.W. Parks, Adaptive homogeneity-directed demosaicing algorithm, IEEE Trans. Image Process. 14 (3) (2005) 360–369.
[35] X. Wu, N. Zhang, Primary-consistent soft-decision color demosaicking for digital cameras (patent pending), IEEE Trans. Image Process. 13 (9) (2004) 1263–1274.
[36] D. Menon, S. Andriani, G. Calvagno, Demosaicing with directional filtering and *a posteriori* decision, IEEE Trans. Image Process. 16 (1) (2007) 132–141.
[37] L. Zhang, X. Wu, Color demosaicking via directional linear minimum mean square-error estimation, IEEE Trans. Image Process. 14 (12) (2005) 2167–2177.
[38] D. Menon, G. Calvagno, Demosaicing based on wavelet analysis of the luminance component, Proceedings of the IEEE International Conference on Image Processing, vol. 2, 2007, pp. 181–184.
[39] D. Paliy, V. Katkovnik, R. Bilcu, S. Alenius, K. Egiazarian, Spatially adaptive color filter array interpolation for noiseless and noisy data, Int. J. Imaging Syst. Technol. 17 (3) (2007) 105–122 (Special Issue on Applied Color Image Processing).
[40] C.-Y. Su, J.-K. Tseng, Demosaicing using variable-size classifiers and proportional weights, in: Proceedings of the IEEE International Conference on Image Processing, 2009, pp. 493–496.
[41] J.S.J. Li, S. Randhawa, Color filter array demosaicking using high-order interpolation techniques with a weighted median filter for sharp color edge preservation, IEEE Trans. Image Process. 18 (9) (2009) 1946–1957.
[42] E. Dubois, The sampling and reconstruction of time-varying imagery with application in video systems, Proceedings of the IEEE 73 (4) (1985) 502–522.
[43] J.W. Glotzbach, R.W. Schafer, K. Illgner, A method of color filter array interpolation with alias cancellation properties, Proceedings IEEE International Conference on Image Processing, vol. 1, 2001, pp. 141–144.
[44] D. Alleysson, S. Süsstrunk, J. Hérault, Linear demosaicing inspired by the human visual system, IEEE Trans. Image Process. 14 (4) (2005) 439–449.
[45] N.-X. Lian, L. Chang, Y.-P. Tan, V. Zagorodnov, Adaptive filtering for color filter array demosaicking, IEEE Trans. Image Process. 16 (10) (2007) 2515–2525.
[46] B. Chaix de Lavarène, D. Alleysson, B. Durette, J. Hérault, Efficient demosaicing through recursive filtering, Proceedings of the IEEE International Conference on Image Processing, vol. 2, 2007, pp. 189–192.
[47] E. Dubois, Frequency-domain methods for demosaicking of Bayer-sampled color images, IEEE Signal Process. Lett. 12 (12) (2005) 847–850.
[48] E. Dubois, Filter design for adaptive frequency-domain Bayer demosaicking, in: Proceedings of the IEEE International Conference on Image Processing, 2006, pp. 2705–2708.
[49] B.K. Gunturk, Y. Altunbasak, R.M. Mersereau, Color plane interpolation using alternating projections, IEEE Trans. Image Process. 11 (9) (2002) 997–1013.
[50] Y.M. Lu, M. Karzand, M. Vetterli, Demosaicking by alternating projections: theory and fast one-step implementation, IEEE Trans. Image Process. 19 (8) (2010) 2085–2098.
[51] X. Li, Demosaicing by successive approximation, IEEE Trans. Image Process. 14 (3) (2005) 370–379.
[52] J. Driesen, P. Scheunders, Wavelet-based color filter array demosaicking, Proceedings of the IEEE International Conference on Image Processing, vol. 5, 2004, pp. 3311–3314.
[53] L. Chen, K.-H. Yap, Y. He, Color filter array demosaicking using wavelet-based subband synthesis, Proceedings of the IEEE International Conference on Image Processing, vol. 2, 2005, pp. 1002–1005.
[54] G. Spampinato, A. Bruna, G. Sanguedolce, E. Ardizzone, M. La Cascia, Improved color interpolation using discrete wavelet transform, Proceedings of the SPIE Image and Video Communications and Processing, vol. 5685, 2005, pp. 753–760.
[55] J. Gu, P.J. Wolfe, K. Hirakawa, Filterbank-based universal demosaicking, in: Proceedings of the IEEE International Conference on Image Processing, 2010, pp. 1981–1984.
[56] D.H. Brainard, Bayesian method for reconstructing color images from thrichromatic samples, in: Proceedings of the IS&T 47th Annual Meeting1994, pp. 375–380.
[57] P. Longere, X. Zhang, P.B. Delahunt, D.H. Brainard, Perceptual assessment of demosaicing algorithm performance, Proc. IEEE 90 (1) (2002) 123–132.
[58] J. Mukherjee, R. Parthasarathi, S. Goyal, Markov random field processing for color demosaicing, Pattern Recognition Lett. 22 (3–4) (2001) 339–351.
[59] Y. Hel-Or, The canonical correlations of color images and their use for demosaicing, Technical Report HPL-2003-164R1, HP Labs Israel, February 2004.
[60] Y. Hel-Or, D. Keren, Demosaicing of color images using steerable wavelets, Technical Report HPL-2002-206R1, HP Labs Israel, August 2002.
[61] D. Taubman, Generalized Wiener reconstruction of images from colour sensor data using a scale invariant prior, Proceedings of the IEEE International Conference on Image Processing, vol. 3, 2000, pp. 801–804.
[62] H.J. Trussell, R.E. Hartwig, Mathematics for demosaicking, IEEE Trans. Image Process. 3 (11) (2002) 485–492.
[63] J. Portilla, D. Otaduy, C. Dorronsoro, Low-complexity linear demosaicing using joint spatial-chromatic image statistics, Proceedings of the IEEE International Conference on Image Processing, vol. 1, 2005, pp. 61–64.
[64] B. Chaix de Lavarène, D. Alleysson, J. Hérault, Practical implementation of LMMSE demosaicing using luminance and chrominance spaces, Comput. Vision Image Understand. 107 (2007) 3–13 Special Issue on Color Image Processing.
[65] G. Demoment, Image reconstruction and restoration: overview of common estimation structures and problems, IEEE Trans. Acoust. Speech Signal Process. 37 (12) (1989) 2024–2036.
[66] W.C. Karl, Regularization in image restoration and reconstruction, in: A. Bovik (Ed.), Handbook of Image and Video Processing, Academic, San Diego, CA 2000, pp. 141–160 (Chapter 3.6).
[67] D. Keren, M. Osadchy, Restoring subsampled color images, Mach. Vision Appl. 11 (4) (1999) 197–202.
[68] S. Farsiu, M. Elad, P. Milanfar, Multiframe demosaicing and super-resolution of color images, IEEE Trans. Image Process. 15 (1) (2006) 141–159.
[69] T. Saito, T. Komatsu, Demosaicing method using the extended color total-variation regularization, Proceedings of the IS&T/SPIE Electronic Imaging: Digital Photography III, vol. 6817, 2008.
[70] L. Condat, A generic variational approach for demosaicking from an arbitrary color filter array, in: Proceedings of the IEEE International Conference on Image Processing, 2009, pp. 1625–1628.
[71] O.A. Omer, T. Tanaka, Image demosaicking based on chrominance regularization with region-adaptive weights, in: International Conference on Information, Communications and Signal Processing, Singapore, 2007, pp. 1–5.
[72] D. Menon, G. Calvagno, A regularization approach to demosaicking, Proceedings of the SPIE-IS&T Electronic Imaging, Visual Communications and Image Processing, vol. 6822, 2008.
[73] D. Menon, G. Calvagno, Regularization approaches to demosaicking, IEEE Trans. Image Process. 18 (10) (2009) 2209–2220.
[74] D.D. Muresan, T.W. Parks, Demosaicing using optimal recovery, IEEE Trans. Image Process. 14 (2) (2005) 267–278.
[75] J. Mairal, M. Elad, G. Sapiro, Sparse representation for color image restoration, IEEE Trans. Image Process. 17 (1) (2008) 53–69.
[76] X. Wu, D. Gao, G. Shi, D. Liu, Color demosaicking with sparse representations, in: Proceedings of the IEEE International Conference on Image Processing2010, pp. 1645–1648.
[77] A. Buades, B. Coll, J. Morel, C. Sbert, Self-similarity driven color demosaicking, IEEE Trans. Image Process. 18 (6) (2009) 1192–1202.
[78] S. Ferrandas, M. Bertalmio, V. Caselles, Geometry-based demosaicking, IEEE Trans. Image Process. 19 (3) (2009) 665–670.
[79] F. Zhang, X. Wu, X. Yang, W. Zhang, L. Zhang, Robust color demosaicking with adaptation to varying spectral correlation, IEEE Trans. Image Process. 18 (12) (2009) 2706–2717.
[80] L. Zhang, X. Wu, Image interpolation via directional filtering and data fusion, IEEE Trans. Image Process. 15 (8) (2006) 2226–2238.
[81] X. Zhang, X. Wu, Image interpolation by adaptive 2-d autoregressive modeling and soft-decision estimation, IEEE Trans. Image Process. 17 (2008) 887–896.
[82] K.H. Chung, Y.H. Chan, A low-complexity joint color demosaicking and zooming algorithm for digital camera, IEEE Trans. Image Process. 16 (7) (2007) 1705–1715.
[83] L. Zhang, D. Zhang, A joint demosaicking-zooming scheme for single sensor digital color cameras, Comput. Vision Image Understand. 107 (2007) 14–25 (Special issue on Color Image Processing).
[84] R. Lukac, K. Martin, K. Plataniotis, Digital camera zooming based on unified cfa image processing steps, IEEE Trans. Consum. Electron. 50 (1) (2004) 15–24.

[85] R. Lukac, K.N. Plataniotis, D. Hatzinakos, Color image zooming on the Bayer pattern, IEEE Trans. Circuits Syst. Video Technol. 15 (11) (2005) 1475–1492.
[86] S.C. Park, M.K. Park, M.G. Kang, Super-resolution image reconstruction: a technical overview, IEEE Signal Process. Mag. 20 (3) (2003) 21–36.
[87] L.I. Rudin, S. Osher, E. Fatemi, Nonlinear total variation based noise removal algorithms, Physica D 60 (1–4) (1992) 259–268.
[88] T. Gotoh, M. Okutomi, Direct super-resolution and registration using raw CFA images, Proceedings of the IEEE International Conference on Computer Vision and Pattern Recognition, vol. 2, 2004, pp. 600–607.
[89] P. Vandewalle, K. Krichane, D. Alleysson, S. Süsstrunk, Joint demosaicing and super-resolution imaging from a set of unregistered aliased images, Proceedings of the IS&T/SPIE Electronic Imaging: Digital Photography III, vol. 6802, 2007.
[90] S.G. Chang, B. Yu, M. Vetterli, Adaptive wavelet thresholding for image denoising and compression, IEEE Trans. Image Process. 9 (9) (2000) 1532–1546.
[91] D.L. Donoho, De-noising by soft-thresholding, IEEE Trans. Inform. Theory 41 (3) (1995) 613–627.
[92] A. Pižurica, W. Philips, Estimating the probability of the presence of a signal of interest in multiresolution single- and multiband image denoising, IEEE Trans. Image Process. 15 (3) (2006) 654–665.
[93] J. Portilla, V. Strela, M.J. Wainwright, E.P. Simoncelli, Image denoising using scale mixtures of Gaussians in the wavelet domain, IEEE Trans. Image Process. 12 (11) (2003) 1338–1351.
[94] O. Kalevo, H. Rantanen, Noise reduction techniques for Bayer-matrix images, Proceedings of the SPIE Sensor and Camera Systems for Scientific, Industrial and Digital Photography Applications III, vol. 4669, 2002.
[95] L. Zhang, R. Lukac, X. Wu, D. Zhang, PCA-based spatially adaptive denoising of CFA images for single-sensor digital cameras, IEEE Trans. Image Process. 18 (4) (2009) 797–812.
[96] K. Hirakawa, T.W. Parks, Joint demosaicing and denoising, IEEE Trans. Image Process. 15 (8) (2006) 2146–2157.
[97] K. Hirakawa, X.-L. Meng, An empirical Bayes EM-wavelet unification for simultaneous denoising interpolation and or demosaicing, in: Proceedings of the IEEE International Conference on Image Processing, 2006, pp. 1453–1456.
[98] K. Hirakawa, X.-L. Meng, P.J. Wolfe, A framework for wavelet-based analysis and processing of color filter array images with applications to denoising and demosaicking, Proceedings of the IEEE International Conference on Acoustics, Speech and Signal Processing, vol. I, 2007, pp. 597–600.
[99] L. Zhang, X. Wu, D. Zhang, Color reproduction from noisy CFA data of single sensor digital cameras, IEEE Trans. Image Process. 16 (9) (2007) 2184–2197.
[100] D. Paliy, A. Foi, R. Bilcu, V. Katkovnik, Denoising and interpolation of noisy Bayer data with adaptive cross-color filters, Proceedings of the SPIE-IS&T Electronic Imaging, Visual Communications and Image Processing, vol. 6822, 2008.
[101] D. Menon, G. Calvagno, Joint demosaicking and denoising with space-varying filters, in: Proceedings of the IEEE International Conference on Image Processing2009, pp. 477–480.
[102] L. Condat, A simple, fast and efficient approach to *denosaicking*: joint demosaicking and denoising, in: Proceedings of the IEEE International Conference on Image Processing2010, pp. 905–908.
[103] X. Zhang, B.A. Wandell, A spatial extension of cielab for digital color-image reproduction, J. Soc. Inf. Disp. 5 (1) (1997) 61–63.
[104] A.B. Poirson, B.A. Wandell, Appearance of colored patterns: pattern-color separability, J. Opt. Soc. Am. 10 (12) (1993) 2458–2470.
[105] A.B. Poirson, B.A. Wandell, Pattern-color separable pathways predict sensitivity to simple colored patterns, Vision Res. 35 (2) (1996) 239–254.
[106] URL: 〈http://www.cipr.rpi.edu/resource/stills/kodak.html〉.